AIAA 2003-5053

The Bidirectional Vortex. Part 2: Viscous Core Corrections

A. B. Vyas and J. Majdalani
Marquette University
Milwaukee, WI 53233

M. J. Chiaverini
Space Center
Orbital Technologies Corporation (ORBITEC)
Madison, WI 53717

39th AIAA/ASME/SAE/ASEE Joint Propulsion Conference and Exhibit
20–23 July 2003
Huntsville, AL

39th AIAA/ASME/SAE/ASEE Joint Propulsion Conference and Exhibit
20-23 July 2003, Huntsville, Alabama

AIAA 2003-5053

The Bidirectional Vortex. Part 2: Viscous Core Corrections

Anand B. Vyas* and Joseph Majdalani†
Marquette University, Milwaukee, WI 53233
and
Martin J. Chiaverini‡
Orbital Technologies Corporation, Madison, WI 53717

This article focuses on the viscous core of the bidirectional flowfield arising in a swirl-driven thrust chamber. By regularizing the momentum equation in the tangential direction, the boundary layer equation that controls the forced vortex near the chamber axis is obtained. After identifying the coordinate transformation needed to resolve the rapid changes near the core, an inner expansion is arrived at. This expansion is then matched with the outer solution associated with the free vortex; the latter is known to prevail in the outer region. By combining inner and outer expansions, uniformly valid approximations are obtained for the swirl velocity, vorticity, and pressure. These are shown to be strongly influenced by a dynamic similarity parameter that combines the mean flow Reynolds number and the chamber aspect ratio. Referred to as the vortex Reynolds number *V*, this dimensionless grouping enables us to quantify the characteristic features of the bidirectional vortex. Among them is the thickness of the viscous core which is found to decrease with the square root of *V*. The converse can be said of the maximum swirl velocity. In the same vein, the angular frequency of the rigid-body rotation of the forced vortex near the core is found to be linearly proportional to *V*. The form of the swirl velocity is reminiscent of the Burgers vortex; here, it is based on the aspect ratio of the thrust chamber. The resulting theoretical predictions compare favorably with experimental measurements and computational results over the length of the chamber.

Nomenclature

a = chamber radius
A_i = inlet area
b = chamber discharge radius
l = chamber aspect ratio, L/a
p = normalized pressure, $\overline{p}/(\rho U^2)$
$\overline{Q}_i$ = inlet volumetric flow rate
Q_i = normalized volumetric flow rate, $\overline{Q}_i/(Ua^2) = \sigma^{-1}$
Re = injection Reynolds number, $Ua/\nu = 1/\varepsilon$
r = normalized radial coordinate, $\overline{r}/a$
S = swirl number, $\pi ab/A_i = \pi\beta\sigma$
$\boldsymbol{u}$ = normalized velocity $(\overline{u}_r, \overline{u}_z, \overline{u}_\theta)/U$
u_θ = normalized swirl/spin/tangential velocity, $\overline{u}_\theta/U$
U = mean inflow velocity, $\overline{u}_\theta(a, L)$
V = vortex Reynolds number, $Q_i Re(a/L) = (\varepsilon\sigma l)^{-1}$
z = normalized axial coordinate, $\overline{z}/a$
β = normalized discharge radius, b/a
$\overline{\delta}$ = radius of the viscous core
δ = normalized core radius, $\overline{\delta}/a$
ε = perturbation parameter, $1/Re = \nu/(Ua)$
κ = inflow parameter, $Q_i/(2\pi l) = (2\pi\sigma l)^{-1}$
ν = kinematic viscosity, μ/ρ
ρ = density
σ = modified swirl number, $Q_i^{-1} = S/(\pi\beta)$

Subscripts
i = inlet property
r = radial component or partial derivative
z = axial component or partial derivative
θ = azimuthal component or partial derivative
= overbars denote dimensional variables

*Graduate student and Research Associate, Department of Mechanical and Industrial Engineering. Member AIAA.
†Assistant Professor, Department of Mechanical and Industrial Engineering. Member AIAA.
‡Lead Propulsion Engineer. Member AIAA.

I. Introduction

IT has long been recognized that the free vortex assumption used to model the swirl velocity in columnar vortices deteriorates in the vicinity of the core (see Harvey[1] and Leibovich[2,3]). This is owed to the tangential (or swirl) velocity in a free vortex being

inversely proportional to the distance measured from the vortex axis. At the outset, a free vortex is known to overpredict both the swirl velocity and the radial pressure gradients in the vicinity of the centerline. In fact, a similar difficulty has been encountered by Long[4] in his classic study of the flow toward a rotating sink.

Despite the adequacy of inviscid formulations in describing the genesis of unidirectional vortices, they have fallen short in capturing important phenomena associated with vortex stability and breakdown. The remedy has been in rescaling the governing equations in order to incorporate the rapid variations that evolve near the core. In the absence of three-dimensional asymmetries, disregarding the wall boundary layer has been shown to be a less important restriction. Near the wall, viscous forces are sufficiently weak that the axial gradient of a flow variable becomes very small in comparison to the radial gradient. Near the core, however, the rescaled equations reveal a forced vortex exhibiting the form suggested by Burgers[5] or Oseen and Hamel.[6] Accordingly, the complete solution must consist of, first, an outer free vortex and, second, an inner forced vortex whose motion resembles solid-body rotation in the core region. This forced vortex incorporates viscous stresses that become important near the axis of the chamber. As a result, the swirl velocity will be led to vanish along the vortex axis instead of growing indefinitely large.

Naturally, bidirectional flows in cyclone separators and combustors have been shown to exhibit analogous core vortex regions (see Lewellen[7]). The bipolar motion is further complicated by the presence of thin Ekman boundary layers at the endwalls (both top and bottom) where the swirl velocity is expected to peak and then decay to zero.[7,8] These layers are often omitted in theoretical analyses due to their small relative sizes and weak impact on the bulk flow motion.

Evidence of a forced vortex near the core of cyclone chambers has actually been reported in the experimental and theoretical studies of Kelsall,[9] Smith,[10,11] Reydon and Gauvin,[12] Ogawa,[13] Lin and Kwok,[14] and Vatistas.[8] More recent contributory experiments and numerical simulations have confirmed the presence of a viscous core using laser-doppler velocimetry (LDV) and computational fluid dynamics (CFD).[15] These studies have shown that the swirl velocity reaches a maximum at a small distance δ from the chamber axis along which it later vanishes. This radial distance is viewed as a representative lengthscale reflecting the size of the core region delineating the forced vortex. Furthermore, δ is found to be invariant along the chamber length. Being observant of conventional boundary layer theory, δ diminishes with successive increases in the Reynolds number.

In a recent theoretical study of the bidirectional flow in a liquid thrust chamber, an (exact) inviscid solution was advanced by Vyas, Majdalani and Chiaverini.[16] This solution was advantageous in its ability to incorporate the axial dependence along the chamber length. It also retained the proper inlet and outlet boundary conditions. Insofar as the thrust chamber resembled an inverted cyclone, the analytical solution agreed favorably with both experimental and numerical predictions of cyclonic flows. It also agreed with previous empirical or semi-analytical correlations that either neglected the axial dependence or relied on basic regression fits. Nonetheless, the analytical solution presented by Vyas, Majdalani and Chiaverini[16] lacked one important ingredient: viscosity. Although viscous interactions did not alter the essential flow character near the sidewalls and endwalls, they mitigated the genesis of a forced vortex near the core. As a result, the swirl velocity and radial pressure gradients became unbounded along the chamber centerline. The extra complication in analyzing this region precluded an exact solution. As suggested by Riley,[17] the ensuing problem could be more efficiently solved numerically.

In this article, a boundary layer treatment of the core region will be pursued. Our analysis will be based on rescaling the momentum equation in the tangential direction. Being the source of singularity, this equation will be, first, regularized by retaining the second order viscous term. Subsequently, it will be solved using the tools of matched asymptotic expansions. In the process of matching, the free vortex will constitute the outer solution. Based on the resulting composite solution, the fundamental flow variables will be re-examined. This will permit the construction of a uniformly valid approximation for the problem at hand. In the process, the swirl velocity and pressure will be made non-singular and the character of the forced vortex will be elucidated.

II. Mathematical Model

Our physical model, nomenclature, normalization, and coordinate system are identical to those adopted by Vyas, Majdalani and Chiaverini.[16] While the overall boundary conditions remain essentially unchanged, the tangential momentum equation is regularized following standard practice (see Balachandar, Buckmaster and Short[18]).

Since $u_\theta \neq u_\theta(\theta, z)$, u_θ does not affect the continuity equation. The axial and radial velocity components u_z and u_r remain as before,[16] related via

$$\frac{1}{r}\frac{\partial (r u_r)}{\partial r} + \frac{\partial u_z}{\partial z} = 0 \quad \text{(continuity)} \tag{1}$$

$$\frac{\partial(u_r\Omega_\theta)}{\partial r}+\frac{\partial(u_z\Omega_\theta)}{\partial z}=0 \text{ (vorticity transport)} \quad (2)$$

$$\frac{\partial u_r}{\partial z}-\frac{\partial u_z}{\partial r}=\Omega_\theta \text{ (vorticity)} \quad (3)$$

with boundary conditions

$$\begin{cases} z=0,\ \forall r,\ u_z=0; \quad r=0,\ \forall z,\ u_r=0 \\ r=1,\ \forall z,\ u_r=0; \quad z=l,\ Q_o=2\pi\int_0^\beta u_z r\,\mathrm{d}r=Q_i \end{cases} \quad (4)$$

As shown before, the solution of this set can be expressed by[16]

$$\boldsymbol{u}=-\kappa\frac{\sin(\pi r^2)}{r}\boldsymbol{e}_r+u_\theta(r)\boldsymbol{e}_\theta+2\pi\kappa z\cos(\pi r^2)\boldsymbol{e}_z;$$

$$\kappa\equiv\frac{Q_i}{2\pi l}=\frac{A_i}{2\pi aL}=\frac{1}{2}\frac{c^2}{a^2}\frac{a}{L}=\frac{1}{2\pi\sigma l}=\frac{1}{2\sqrt{2}Sl} \quad (5)$$

In order to suppress the singular behavior exhibited by the swirl velocity, the second order viscous term must be retained in the tangential momentum equation. The resulting dimensionless relation can be written as

$$u_r\frac{\partial u_\theta}{\partial r}+\frac{u_r u_\theta}{r}=\frac{1}{Re}\frac{\partial}{\partial r}\left[\frac{1}{r}\frac{\partial(ru_\theta)}{\partial r}\right];\ Re\equiv\frac{Ua}{\nu} \quad (6)$$

where Re is the mean flow Reynolds number. In cyclone separators and combustors, Re is of order 10^5. Recalling that $u_\theta=u_\theta(r)$, Eq. (6) reduces to an ordinary differential equation (ODE), namely,

$$u_r\frac{\mathrm{d}u_\theta}{\mathrm{d}r}+\frac{u_r u_\theta}{r}=\varepsilon\frac{\mathrm{d}}{\mathrm{d}r}\left[\frac{1}{r}\frac{\mathrm{d}(ru_\theta)}{\mathrm{d}r}\right];\ \varepsilon\equiv\frac{1}{Re} \quad (7)$$

The two boundary conditions are due to the forced vortex requirement at the core and to the tangential inflow at entry. These translate into

$$\begin{cases} r=0,\ \forall z,\ u_\theta=0 \\ r=1,\ z=l,\ u_\theta=1 \end{cases} \quad (8)$$

Based on Eq. (5), one can put

$$-\frac{\kappa}{r}\sin(\pi r^2)\frac{\mathrm{d}u_\theta}{\mathrm{d}r}-\frac{\kappa}{r^2}\sin(\pi r^2)u_\theta=\varepsilon\frac{\mathrm{d}}{\mathrm{d}r}\left[\frac{1}{r}\frac{\mathrm{d}(ru_\theta)}{\mathrm{d}r}\right] \quad (9)$$

and so

$$\varepsilon\frac{\mathrm{d}}{\mathrm{d}r}\left[\frac{1}{r}\frac{\mathrm{d}(ru_\theta)}{\mathrm{d}r}\right]+\frac{\kappa}{r^2}\sin(\pi r^2)\frac{\mathrm{d}(ru_\theta)}{\mathrm{d}r}=0 \quad (10)$$

Both terms can now be divided by r; one gets

$$\varepsilon\frac{1}{r}\frac{\mathrm{d}}{\mathrm{d}r}\left[\frac{1}{r}\frac{\mathrm{d}(ru_\theta)}{\mathrm{d}r}\right]+\frac{\kappa}{r^2}\sin(\pi r^2)\left[\frac{1}{r}\frac{\mathrm{d}(ru_\theta)}{\mathrm{d}r}\right]=0 \quad (11)$$

Equation (11) can be shortened using

$$\eta\equiv\tfrac{1}{2}r^2;\quad \xi\equiv ru_\theta \quad (12)$$

thus yielding,

$$\varepsilon\frac{\mathrm{d}^2\xi}{\mathrm{d}\eta^2}+\kappa\frac{\sin(2\pi\eta)}{2\eta}\frac{\mathrm{d}\xi}{\mathrm{d}\eta}=0 \quad (13)$$

III. Solution

In practical applications, the mean flow Reynolds number is of order 1000 or more. The parameter ε arising in Eq. (13) becomes increasingly smaller and can hence be used as a perturbation parameter. As ε tends to zero, the nature of the equation changes drastically. Specifically, it turns into a first order ODE. The singularity associated with a small parameter multiplying the highest derivative is commensurate with a boundary layer type behavior. Accordingly, the solution is expected to behave differently in two distinct regions. In the outer region, the role of ε is expected to be small. In the inner region, however, the second order diffusion term becomes as large as the convective term arising in Eq. (13). Pursuant to conventional asymptotic theory, a separate expansion needs to be sought in each region. A complete solution could then be arrived at by ensuring that the inner expansion would match the outer expansion in the overlap region. The uniformly valid formulation would then consist of the sum of inner and outer expansions minus their common overlap value.

A. Outer Expansion

The behavior in the outer region can be captured at leading order by setting $\varepsilon=0$ and solving the resulting differential equation. Using $\xi_o=\xi_o^{(0)}+\varepsilon\xi_o^{(1)}+\ldots$, one obtains

$$\frac{\kappa}{2\eta}\sin(2\pi\eta)\frac{\mathrm{d}\xi_o^{(0)}}{\mathrm{d}\eta}=0;\quad \xi_o^{(0)}=\text{constant}=C_0 \quad (14)$$

where the subscript 'o' denotes an outer expansion. It is reassuring to note that the zeroth order solution corresponds to the free vortex $\xi_o^{(0)}=ru_\theta^{(0)}=C_0$ obtained previously.[16]

B. Inner Expansion

To explore the solution near the core, it is necessary to stretch the region around the axis of the chamber. This can be accomplished by introducing the radial coordinate transformation

$$s=\frac{\eta}{\delta(\varepsilon)} \quad (15)$$

Using the subscript 'i' to designate the inner solution, the spatial distortion associated with Eq. (15) can be employed in Eq. (13); one finds,

$$\frac{\varepsilon}{\delta^2}\frac{\mathrm{d}^2\xi_i}{\mathrm{d}s^2}+\frac{\kappa}{2s\delta^2}\sin(2\pi s\delta)\frac{\mathrm{d}\xi_i}{\mathrm{d}s}=0 \quad (16)$$

and so

$$\frac{\mathrm{d}^2\xi_i}{\mathrm{d}s^2}+\frac{\kappa}{2\varepsilon s}\sin(2\pi s\delta)\frac{\mathrm{d}\xi_i}{\mathrm{d}s}=0 \quad (17)$$

Owing to the importance of both diffusive and convective acceleration terms near the core, the two terms in Eq. (17) will be of the same order if, and only

if, the coefficient of the first derivative remains bounded for all ε. This statement translates into

$$\frac{\kappa}{2\varepsilon s}\sin(2\pi s\delta)=\frac{\kappa}{2\varepsilon s}\left(2\pi s\delta-\tfrac{4}{3}\pi^3 s^3\delta^3+\ldots\right)=O(1) \quad (18)$$

The proper scaling transformation must hence be chosen such that $\delta/\varepsilon=O(1)$. At the outset, one deduces the distinguished limit to be

$$\delta(\varepsilon)\sim\varepsilon \quad (19)$$

Without loss in generality, one may choose $\delta(\varepsilon)=\varepsilon$ and substitute back into Eq. (18). Forthwith, the variable coefficient expressed in the inner variable reduces to

$$\kappa\frac{\sin(2\pi\varepsilon s)}{2\varepsilon s}=\kappa\left[\pi+O(\varepsilon^2)\right] \quad (20)$$

Using a series of the form $\xi_i=\xi_i^{(0)}+\varepsilon\xi_i^{(1)}+\ldots$, one may determine each successive viscous correction after revisiting Eq. (17). At leading order, the inner equation becomes

$$\frac{\mathrm{d}^2\xi_i^{(0)}}{\mathrm{d}s^2}+\pi\kappa\frac{\mathrm{d}\xi_i^{(0)}}{\mathrm{d}s}=0 \quad (21)$$

Consequently,

$$\xi_i^{(0)}=K_0-\frac{K_1}{\pi\kappa}\exp(-\pi\kappa s) \quad (22)$$

C. Asymptotic Matching

Prandtl's matching principle can now be utilized to reconcile the inner and outer expansions at leading order. The matching criterion may be expressed as

$$\lim_{s\to\infty}\ \xi_i^{(0)}=\lim_{\eta\to 0}\ \xi_o^{(0)} \quad (23)$$

hence,

$$\lim_{s\to\infty}K_0-\frac{K_1}{\pi\kappa}\exp(-\pi\kappa s)=\lim_{\eta\to 0}\ C_0=\xi_{cl} \quad (24)$$

where ξ_{cl} represents the common limit. After deducing that $\xi_{cl}=K_0=C_0$, the composite expansion can be arrived at by combining

$$\xi_c=\xi_o+\xi_i-\xi_{cl} \quad (25)$$

After some cancellations, ξ_c collapses into

$$\xi_c=K_0-\frac{K_1}{\pi\kappa}\exp\left(-\pi\kappa\frac{\eta}{\varepsilon}\right) \quad (26)$$

When reverting to original coordinates, ξ_c and η are exchanged by ru_θ and $\frac{1}{2}r^2$, respectively. The uniformly valid approximation for u_θ is thus obtained, namely,

$$u_\theta=\frac{K_0}{r}\left[1-\frac{K_1}{\pi\kappa K_0}\exp\left(-\pi\kappa\frac{r^2}{2\varepsilon}\right)\right] \quad (27)$$

D. Complete Solution

As the first boundary condition in Eq. (8) requires a zero swirl velocity at the core, one must have

$$\frac{K_1}{\pi\kappa K_0}=1 \text{ or } K_0=\frac{K_1}{\pi\kappa} \quad (28)$$

Substituting this constant into Eq. (27), an expression similar to Burger's vortex is realized. One finds

$$u_\theta=\frac{K_1}{\pi\kappa r}\left[1-\exp(-\pi\kappa r^2/2\varepsilon)\right] \quad (29)$$

The last constant K_1 may be determined from the velocity boundary condition requiring that the velocity at the wall be the same as the injection velocity,

$$\frac{K_1}{\pi\kappa}\left[1-\exp\left(-\pi\kappa/2\varepsilon\right)\right]=1 \quad (30)$$

or

$$K_1=\pi\kappa/\left\{\left[1-\exp\left(-\pi\kappa/2\varepsilon\right)\right]\right\} \quad (31)$$

Substituting K_1 into Eq. (29), and using $\kappa=Q_i/(2\pi l)$, one finally gathers

$$u_\theta=\frac{1-e^{-Q_i r^2/(4\varepsilon l)}}{r\left[1-e^{-Q_i/(4\varepsilon l)}\right]}=\frac{1-e^{-r^2/(4\varepsilon\sigma l)}}{r\left[1-e^{-1/(4\varepsilon\sigma l)}\right]} \quad (32)$$

Note that as $\varepsilon\to 0$, the swirl velocity associated with a free vortex is recovered, namely, $u_\theta=1/r$. Conversely, as $r\to 0$ at fixed ε, one can expand Eq. (32) into

$$u_\theta=\frac{Q_i r[1-\frac{1}{8}Q_i r^2/(\varepsilon l)+\frac{1}{96}r^4Q_i^2/(\varepsilon^2 l^2)+\ldots]}{4\varepsilon l\left[1-e^{-Q_i/(4\varepsilon l)}\right]}$$
$$=\frac{r[1-\frac{1}{8}r^2/(\varepsilon\sigma l)+\frac{1}{96}r^4/(\varepsilon^2\sigma^2 l^2)+\ldots]}{4\varepsilon\sigma l\left[1-e^{-Q_i/(4\varepsilon l)}\right]} \quad (33)$$

This expansion enables us to restore the forced vortex form $u_\theta=\omega r$ where

$$\omega\sim\frac{Q_i}{4\varepsilon l\left[1-e^{-Q_i/(4\varepsilon l)}\right]}=\frac{1}{4\varepsilon\sigma l\left[1-e^{-1/(4\varepsilon\sigma l)}\right]} \quad (34)$$

Clearly, ω represents the angular speed of the core layer which, due to concentrated viscous stresses, is compelled to rotate as a rigid body about the chamber axis.

E. A Modified Reynolds Number

It may be worthwhile mentioning that the solution is markedly controlled by a dynamic similarity parameter that combines ε, σ and the chamber aspect ratio l. By virtue of l being accounted for in this study, it appears that the bidirectional flowfield is strongly influenced by the ratio of the mean flow Reynolds number and the product of the modified swirl number and chamber aspect ratio. As suggested by the current expression for u_θ, the swirl velocity is controlled by an effective Reynolds number,

$$V\equiv\frac{1}{\varepsilon\sigma l}=\frac{Re}{\sigma}\frac{a}{L}=Re\frac{\bar{Q}_i}{Ua^2}\frac{a}{L}=\frac{\bar{Q}_i}{L\nu} \quad (35)$$

To the extent that the finite chamber length is quintessential to the existence of the bidirectional

vortex, the modified Reynolds number based on the chamber aspect ratio and modified swirl number will be referred to, hereafter, as the vortex Reynolds number V. When expressed in terms of V, the swirl velocity becomes

$$u_\theta = \frac{1-e^{-\frac{1}{4}Vr^2}}{r(1-e^{-\frac{1}{4}V})} \tag{36}$$

Similarly, the angular speed of the core reduces to

$$\omega \sim \frac{V}{4(1-e^{-\frac{1}{4}V})} \tag{37}$$

F. Uniformly Valid Pressure Distribution

Now that the swirl velocity is no longer singular at the core, a reassessment of the radial component of the pressure gradient is necessary. Forthwith, the pressure gradient can be re-derived from the classic Euler equation. After some effort, one finds

$$\frac{\partial p}{\partial r} = \frac{1}{r^3}\left(1-e^{-Vr^2/4}\right)^2\left(1-e^{-V/4}\right)^{-2} + \kappa^2 r^{-3}\sin(\pi r^2)\left[\sin(2\pi r^2) - 2\pi r^2\cos(2\pi r^2)\right] \tag{38}$$

While the axial pressure gradient remains unchanged, partial integration of the pressure gradient permits obtaining an expression for the pressure distribution along the chamber length. After some symbolic programming, one finds

$$p = p_0 + \kappa^2\frac{\cos(2\pi r^2) - 8\pi^2 r^2 z^2}{4r^2} - \frac{\left\{\kappa^2(1+e^{-\frac{1}{2}V} - 2e^{-\frac{1}{4}V}) / 4r^2(1-e^{-\frac{1}{4}V})^2 + 2 + 2e^{-\frac{1}{2}Vr^2} - 4e^{-\frac{1}{4}Vr^2} + r^2 V\left[\mathrm{Ei}(-\tfrac{1}{2}Vr^2) - \mathrm{Ei}(-\tfrac{1}{4}Vr^2)\right]\right\}}{} \tag{39}$$

Here $\mathrm{Ei}(x)$ refers to the second exponential integral function given by Abramowitz and Stegun.[19] Specifically, one defines

$$\mathrm{Ei}(x) = \gamma + \ln|x| + \sum_{m=1}^{\infty}\frac{1}{m!m}x^m \tag{40}$$

where $\gamma = 0.5772156649$ is Euler's constant.

IV. Discussion

Inclusion of viscosity in the tangential momentum balance has an appreciable impact on the swirl velocity, mean flow vorticity, and radial pressure gradient. Viscosity also affects the radial thickness of the forced vortex which does not seem to vary along the length of the chamber. These features will now be examined, starting with the swirl velocity.

A. Swirl Velocity

According to Eq. (32), the tangential component of the velocity starts at the wall with a value that matches the distributed injection velocity at the base. It then increases to a maximum that delimits the envelope inside which viscous forces begin to dominate. After passing through this maximum $(u_\theta)_{\max}$, the swirl velocity begins to depreciate gradually until it reaches zero at the chamber centerline.

A plot of u_θ is given in Fig. 1 at three different vortex Reynolds numbers of 10^2, 10^3, and 10^4. Note that increasing the chamber aspect ratio is paramount to magnifying the role of viscosity due to the impact of the chamber aspect ratio on the solution by way of the vortex Reynolds number V.

As shown on the graph, the radius of the forced vortex expands with successive increases in viscosity. It is largest at the smallest value of V. As the vortex Reynolds number is increased to 10^4, the point of maximum swirl draws nearer to the core. This behavior is accompanied by an increase in the magnitude of $(u_\theta)_{\max}$. With further increases in the vortex Reynolds number, it is clear that u_θ approaches the inviscid limit by becoming very large near the centerline. The boundary layer curves shown in Fig. 1 appear to be in agreement with experimental measurements acquired by Vatistas and co-workers.[8,14] They also seem to agree fairly well with both CFD and LDV predictions

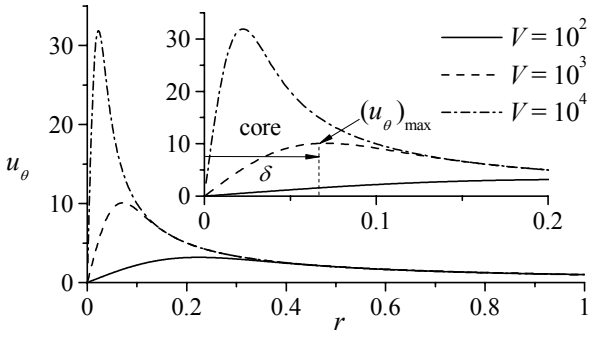

Fig. 1 Swirl velocity versus $V = \bar{Q}_i/(L\nu)$.

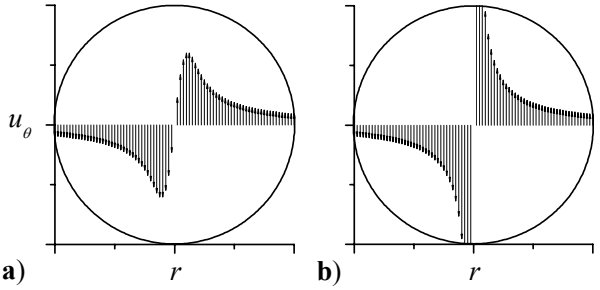

Fig. 2 Typical vector plot of the swirl velocity using a) the viscous forced vortex model near the core and b) the inviscid free vortex model throughout the chamber.

obtained recently by Hoekstra, Derksen and Van den Akker.[15] A two-dimensional vector plot of the swirl velocity is shown in Figs. 2a and 2b with and without viscous corrections, respectively. The breakdown of the free vortex model in Fig. 2b leads to unrealistically large velocity amplitudes in the vicinity of the core.

B. Viscous Core Thickness

In order to quantify the forced vortex region, it is helpful to select a characteristic lengthscale that would be commensurate with the size of the rigid-body, irrotational flow region in which viscous forces are appreciable. For this purpose, we choose the radial distance to $(u_\theta)_{\max}$ as our characteristic length δ. As shown in the inset of Fig. 1, this distance extends from the chamber axis to the center of the overlap region where the outer and inner solutions merge. Since the inner region is confined to $0 \le r \le \delta$, the diameter of the forced vortex may be chosen, as usual, to be twice this distance, specifically, 2δ.

In order to proceed, one must realize that $\delta = r_{\max}$ where $r_{\max}$ must be derived from the root of

$$\left.\frac{\mathrm{d}u_\theta}{\mathrm{d}r}\right|_{r_{\max}} = 0 \tag{41}$$

Differentiating Eq. (32) yields

$$\left.\frac{\mathrm{d}u_\theta}{\mathrm{d}r} = \frac{\left[Vr^2+2\right]e^{-\frac{1}{4}Vr^2} - 2}{2r^2\left[1-e^{-\frac{1}{4}V}\right]}\right|_{r=r_{\max}} = 0 \tag{42}$$

which, in turn, leaves us with

$$\left[Vr_{\max}^2+2\right]e^{-\frac{1}{4}Vr_{\max}^2} - 2 = 0 \tag{43}$$

Fortuitously, an exact root to this transcendental relation can be extracted. One finds

$$r_{\max} = \sqrt{2\left[-1-2\,\mathrm{pln}\left(-1,-\tfrac{1}{2}e^{-\frac{1}{2}}\right)\right]/V} \tag{44}$$

where $\mathrm{pln}(x,y)$ represents the product log function. At the outset, the radius of the forced vortex is hence expressible by

$$\delta = r_{\max} = 2.24181/V^{\frac{1}{2}} \tag{45}$$

Clearly, the thickness of the viscous core is inversely proportional to the square root of the vortex Reynolds number. This result is typical of boundary layers in steady, non-swirling flows.

A plot of δ versus V is now given in Fig. 3. This curve also represents the locus of the maximum swirl velocity. Its invariance with the axial coordinate may be ascribed to the neglect of thin Ekman-type layers forming along the endwalls.

Equation (44) permits calculating the maximum swirl velocity for an arbitrary inlet area ratio, chamber aspect ratio, swirl number, and mean flow Re. In fact, backward substitution into Eq. (32) gives

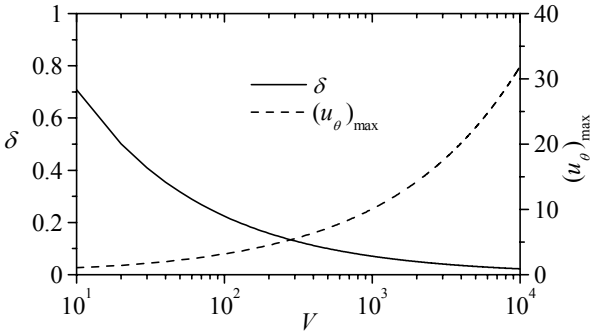

Fig. 3 Maximum swirl speed and its locus versus V.

$$(u_\theta)_{\max} = \frac{\left\{1-\exp\left[\tfrac{1}{2}+\mathrm{pln}\left(-1,-\tfrac{1}{2}e^{-\frac{1}{2}}\right)\right]\right\}\sqrt{V}}{\left[1-e^{-\frac{1}{4}V}\right]\sqrt{\left[-1-2\,\mathrm{pln}\left(-1,-\tfrac{1}{2}e^{-\frac{1}{2}}\right)\right]}}$$
$$= \frac{0.319086\sqrt{V}}{\left[1-e^{-\frac{1}{4}V}\right]} \cong \frac{0.3191V^{\frac{1}{2}}}{(1-e^{-\frac{1}{4}V})} \tag{46}$$

A plot of $(u_\theta)_{\max}$ versus V is added to Fig. 3. Clearly, the maximum swirl velocity increases with successive increases in the vortex Reynolds number. This is due to the driving swirl speed at entry being a) entirely tangential, and b) directly proportional to the vortex Reynolds number.

C. Vorticity Correction

The region corresponding to $0 \le r \le \delta$ is the viscous core flanked circumferentially by an outer field that is largely inviscid. Flow rotationality in the outer region is slightly altered due to viscous interactions with the forced vortex. In fact, a reassessment of vorticity leads to

$$\boldsymbol{\Omega} = 4\pi^2\kappa rz\sin(\pi r^2)\boldsymbol{e}_\theta + \frac{V\exp(-\frac{1}{4}Vr^2)}{2[1-\exp(-\frac{1}{4}V)]}\boldsymbol{e}_z \tag{47}$$

By way of verification, it may be helpful to note that, as $\varepsilon \to 0$, the vorticity of the inviscid solution is restored.[16] A plot of the axial-to-total vorticity is given in Fig. 4 to illustrate the accelerated decay of the viscous-induced Ω_z at larger V. These results are shown in Fig. 4a across the chamber radius for $z/l = 1$ and several values of V and σ. As illustrated in Fig. 4b, we find the dependence on z/l to be marginal except for very low V .or when approaching the head end. In that vicinity, vorticity is everywhere dominated by its axial component. Near the base, however, the converse is true, especially as one approaches the centerline.

In reference to Eq. (33), the near-core motion is prescribed by a linear relation between the swirl velocity and the radial coordinate as $r \to 0$. Being of

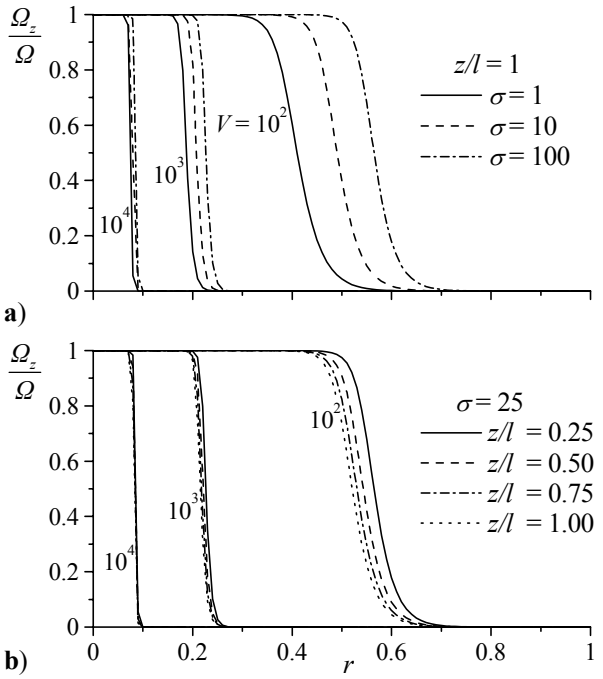

Fig. 4 Axial-to-total vorticity shown a) at the chamber aft end for select values of V and σ, and b) at equispaced chamber locations for select values of V and fixed $\sigma = 25$.

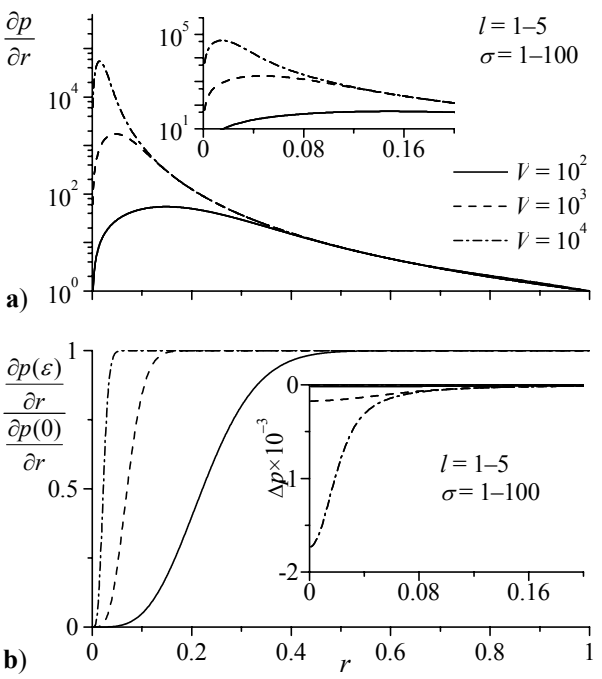

Fig. 5 Radial variation at select values of V and l for a) the pressure gradient, and b) the pressure gradient referenced to its inviscid value. The inset in b) illustrates the pressure variation at the head end.

the form $u_\theta = \omega r$, the angular speed of the forced vortex can be estimated from Eq. (37). Accordingly, so long as $V > 10$, one can put $\omega = V/4$.

D. Pressure Correction

The pressure distribution and its radial gradient are illustrated at the head end in Fig. 5. From the graph, one infers that the pressure drop increases with the radial coordinate. The pressure distribution in the axial direction is almost negligible when compared to the rapid radial variations. With the advent of viscous corrections, the pressure gradient in Fig. 5a passes through a maximum as one approaches the core. This peak can be calculated from Eq. (38). The pressure peak shown in Fig. 5a increases in magnitude and moves closer to the axis of the chamber when V is increased. This behavior is, of course, consistent with a forced vortex.

When the radial pressure gradient is normalized by its inviscid value in Fig. 5b, it is found to be virtually independent of l or σ; instead, it remains a strong function of V. The same can be said of the total pressure which is shown in the inset of Fig. 5b.

The total pressure can be normalized by its maximum radial value $p(1,0)$ taken at the head-end wall. The results are shown in Fig. 6 alongside experimental measurements acquired in a cold-flow

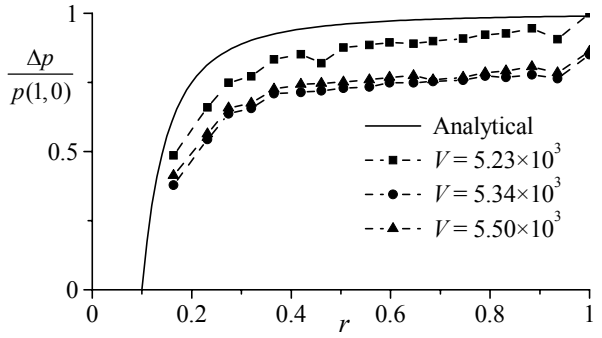

Fig. 6 Comparison between analytical and experimental measurements acquired at the chamber head end. The experiment is based on a cold-flow set-up using water as the working fluid.

apparatus using water as the working fluid. Despite the small variability in the vortex Reynolds number employed in the experiment, the data scatter seems to be consistent with increasing V. For the small variation in V from 5.23×10^3 to 5.50×10^3, the analytical solution remains graphically the same. The agreement with the cold-flow results is reassuring especially that the range of V used in the experiment is typical of that associated with industrial cyclones and swirl burners.

Based on Eq. (38), one can calculate the radial distance δ_p corresponding to the point of maximum $\partial p/\partial r$. Starting with

$$\left.\frac{\mathrm{d}}{\mathrm{d}r}\left(\frac{\partial p}{\partial r}\right)\right|_{r_{\max}} = 0 \tag{48}$$

an asymptotic expression for $\delta_p = r_{\max}$ can be obtained, specifically

$$\delta_p \cong 1.48351/V^{\frac{1}{2}} \tag{49}$$

The relative error associated with Eq. (49) is negligible, being less than $0.037\,\%$ for $V \geq 100, \sigma \geq 1$ and less than $3.5\times10^{-5}\,\%$ for $V \geq 100, \sigma \geq 25$. This error drop precipitously with increasing V or σ. Note that the maximum radial pressure gradient is closer to the core than the maximum swirl velocity. This is due to

$$\delta_p/\delta \cong 0.662 \tag{50}$$

In view of $\delta_p \sim \delta \sim V^{-1/2}$, the thickness of the viscous core is confirmed to be inversely proportional to $V^{1/2}$.

Having determined δ_p, the corresponding pressure gradient can be evaluated from

$$\left.\frac{\partial p}{\partial r}\right|_{\max} = \frac{0.0548466V^{3/2}}{[1-\exp(-\frac{1}{2}V)]^2} \cong 0.0548466V^{3/2} \tag{51}$$

The relative error in Eq. (51) is insignificant, namely, below $0.137\,\%$ for $V \geq 100, \sigma \geq 1$ and below $0.069\,\%$ for $V \geq 100, \sigma \geq 25$. Both δ_p and the maximum radial pressure gradient are plotted in Fig. 7.

V. Concluding Remarks

In this article, a viscous correction is applied to the bidirectional vortex appropriate of an idealized swirl-driven liquid propellant thrust chamber. The viscous correction prevents the swirl velocity and pressure from becoming unbounded along the centerline.

Based on the analytical results, the thickness of the forced vortex is characterized as function of the chamber aspect ratio, the swirl number, and the flow Reynolds number. In fact, one finds the viscous core to decrease with the square root of the vortex Reynolds number, a byproduct of the mean flow Reynolds number, the swirl number, and the chamber aspect ratio. When the kinematic viscosity or the chamber length are increased, the diameter of the forced vortex is magnified proportionately with $\delta \sim V^{-1/2}$. Being proportional to $\nu^{\frac{1}{2}} L^{\frac{1}{2}} \bar{Q}_i^{-\frac{1}{2}}$, the core thickness increases when the chamber length is increased, the viscosity is increased, and when the injected volumetric flow rate is reduced.

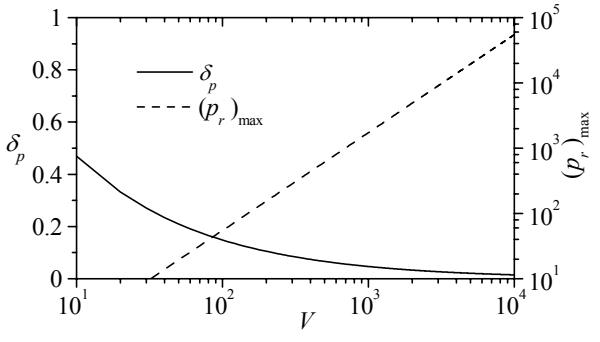

Fig. 7 Maximum radial pressure gradient and its locus versus V.

The inclusion of viscous forces leads to damping of the swirl velocity which now reduces to zero at the centerline. The same trend is exhibited by the pressure and its radial gradient. Friction near the axis also engenders a small non-zero axial vorticity component that vanishes as the sidewall is approached. Due to the tighter packing in the inner region, the viscous core is forced to rotate as a solid cylinder with an average angular speed of $\omega \sim \delta^{-2} \sim V$. Being proportional to $\bar{Q}_i \nu^{-1} L^{-1}$, the angular frequency of the forced vortex increases by increasing the volumetric flow rate. It also increases in shorter motors with smaller viscosity. These results help illuminate the bidirectional flow characteristics and increase our repertory of analytical approximations for confined swirling motions.

Acknowledgments

The first two authors gratefully acknowledge the support received from NASA and the Wisconsin Space Grant Consortium. We are especially thankful for the direction and management of R. Aileen Yingst, Sharon D. Brandt, Steven I. Dutch, and Thomas H. Achtor. The authors also wish to thank William H. Knuth, Ronald R. Teeter, and Eric E. Rice of Orbital Technologies Corporation; their additional support is greatly appreciated.

References

[1]Harvey, J. K., "Some Observations of the Vortex Breakdown Phenomenon," *Journal of Fluid Mechanics,* Vol. 14, 1962, pp. 585-592.

[2]Leibovich, S., "The Structure of Vortex Breakdown," *Annual Review of Fluid Mechanics*, Vol. 101978, pp. 221-246.

[3]Leibovich, S., "Vortex Stability and Breakdown: Survey and Extension," *AIAA Journal,* Vol. 22, No. 9, 1984, pp. 1192-1206.

[4]Long, R. R., "Sources and Sinks at the Axis of a Rotating Liquid," *Quarterly Journal of Mechanics and Applied Mathematics,* Vol. 9, 1956, pp. 385-399.

[5]Burgers, J. M., "A Mathematical Model Illustrating the Theory of Turbulence," *Advances in Applied Mechanics,* Vol. 1, 1948, pp. 171-196.

[6]Schlichting, H., *Boundary-Layer Theory*, 7th ed., McGraw-Hill Book Company Inc., New York, 1979.

[7]Lewellen, W. A., "A Review of Confined Vortex Flows," NASA, Technical Rept. CR-1772, July 1971.

[8]Vatistas, G. H., "Tangential Velocity and Static Pressure Distributions in Vortex Chambers," *AIAA Journal,* Vol. 25, No. 8, 1987, pp. 1139-1140.

[9]Kelsall, D. F., "A Study of Motion of Solid Particles in a Hydraulic Cyclone," *Transactions of the Institution of Chemical Engineers,* Vol. 30, 1952, pp. 87-103.

[10]Smith, J. L., "An Experimental Study of the Vortex in the Cyclone Separator," *Journal of Basic Engineering-Transactions of the ASME*, 1962, pp. 602-608.

[11]Smith, J. L., "An Analysis of the Vortex Flow in the Cyclone Separator," *Journal of Basic Engineering-Transactions of the ASME*, 1962, pp. 609-618.

[12]Reydon, R. F., and Gauvin, W. H., "Theoretical and Experimental Studies of Confined Vortex Flow," *The Canadian Journal of Chemical Engineering,* Vol. 59, 1981, pp. 14-23.

[13]Ogawa, A., "Estimation of the Collection Efficiencies of the Three Types of the Cyclone Dust Collectors from the Standpoint of the Flow Pattern in the Cylindrical Cyclone Dust Collectors," *Bulletin of the JSME,* Vol. 27, No. 223, 1984, pp. 64-69.

[14]Vatistas, G. H., Lin, S., and Kwok, C. K., "Theoretical and Experimental Studies on Vortex Chamber Flows," *AIAA Journal,* Vol. 24, No. 4, 1986, pp. 635-642.

[15]Hoekstra, A. J., Derksen, J. J., and Van den Akker, H. E. A., "An Experimental and Numerical Study of Turbulent Swirling Flow in Gas Cyclones," *Chemical Engineering Science,* Vol. 54, 1999, pp. 2055-2065.

[16]Vyas, A. B., Majdalani, J., and Chiaverini, M. J., "The Bidirectional Vortex. Part 1: An Exact Inviscid Solution," AIAA Paper 2003-5052, July 2003.

[17]Riley, N., "High Reynolds Number Flows with Closed Streamlines," *Journal of Engineering Mathematics,* Vol. 15, 1981, pp. 15-29.

[18]Balachandar, S., Buckmaster, J. D., and Short, M., "The Generation of Axial Vorticity in Solid-Propellant Rocket-Motor Flows," *Journal of Fluid Mechanics,* Vol. 429, 2001, pp. 283-305.

[19]Abramowitz, M., and Stegun, I. A., *Handbook of Mathematical Functions*, National Bureau of Standards, New York, 1964.